Contrast formation in atomic resolution scanning force microscopy on CaF_2(111): experiment and theory

2001 J. Phys.: Condens. Matter 13 2061

(http://iopscience.iop.org/0953-8984/13/10/303)

INSTITUTE OF PHYSICS PUBLISHING JOURNAL OF PHYSICS: CONDENSED MATTER

J. Phys.: Condens. Matter **13** (2001) 2061–2079 www.iop.org/Journals/cm PII: S0953-8984(01)19117-4

Contrast formation in atomic resolution scanning force microscopy on $CaF_2(111)$: experiment and theory

C Barth[1], A S Foster[2], M Reichling[1] and A L Shluger[3]

[1] Department Chemie, Universität München, Butenandtstrasse 5-13, 81377 München, Germany
[2] Laboratory of Physics, Helsinki University of Technology, PO Box 1100, 02015 HUT, Finland
[3] Department of Physics and Astronomy, University College London, Gower Street, London WC1E 6BT, UK

E-mail: reichling@cup.uni-muenchen.de (M Reichling) and a.shluger@ucl.ac.uk (A L Shluger)

Received 14 November 2000, in final form 4 January 2001

Abstract

We investigate mechanisms of contrast formation in atomic resolution imaging of flat terraces on the $CaF_2(111)$ surface with scanning force microscopy operated in the dynamic mode. Experimental results are interpreted with a theory based on atomistic modelling. Experiments reveal characteristic contrast features in the form of triangles that can be explained by theory as being due to the interaction of a positively terminated tip with fluorine ions from two different sublattices. Results for a tip with negative termination are found not to be compatible with experiments. We demonstrate that theory correctly predicts the trend in contrast changes when varying the tip–surface distance but is also limited in quantitative agreement due to the non-ideal atomic structure of real tips. In a distance range where such peculiarities do not play a major role, however, we find good quantitative agreement between theoretical predictions and experimental results. The validity of the comparison between theory and experimental scan lines is discussed in detail using an extensive statistical image analysis.

1. Introduction

Atomic resolution characterization of structures and defects on surfaces of bulk inorganic insulators and poorly conducting materials is of great interest in various fields of science and engineering since the functionality of such materials often critically depends on the surface structure on the atomic scale. As examples, we mention fluoride surfaces gaining tremendous importance for ultraviolet optical components and oxide surfaces that are widely used as supports for catalysts. Surface structure and defects strongly influence optical performance and radiation stability of the former [1], while they determine nucleation, growth and stability of catalytically active particles for the latter [2]. The only direct analytical technique allowing surface analysis of insulators on the atomic scale available to date is scanning force microscopy (SFM) operated in the dynamic mode [3]. Recent progress in developing this technique

has made it possible to obtain high-resolution images on fluoride [4] and oxide [5] surfaces. Atomic resolution has been obtained across steps on CaF_2(111) [6] and NaCl films grown on Cu(111) [7]. The surface reconstruction and related features have been studied extensively on the (110) surface of titanium dioxide [8].

These and similar studies mostly produce unique results, rarely reproduced by other laboratories. Standard procedures for reliably measuring specific surface structures and quantitative understanding of the observed atomic scale contrast features are still lacking. One of the prerequisites for a quantitative understanding is a reliable theory that is able to predict and reproduce the details of atomic structures observed experimentally. Significant progress in theoretical modelling of SFM imaging of ionic surfaces allowed us to elucidate the nature of the image contrast, and to study the influence of tip composition and atomic relaxation during scanning [9–11]. The comparison of theoretical results with experiments is, however, still in its early stages [7] and the interpretation of SFM images is far from being quantitative.

We consider the present paper as a further step towards quantitative analysis and understanding of SFM images of ionic insulators. We performed a systematic cooperative study involving experimental measurements and extensive theoretical modelling of an atomically flat (111) surface of a cleaved CaF_2 crystal. This is a prototype fluoride material that has also been investigated in our previous studies [4, 6]. Recently we have shown that, by combining experiment and theory and analysing subtle features observed in atomically resolved SFM images, it is possible to distinguish whether fluorine or calcium ions have been imaged as bright [12]. The aim of the present work is to systematically extend this approach and to use statistical analysis of experimental data and comparison between theory and experiment to explore the possibility of a unique quantitative characterization of observed images.

The paper is organized as follows. After introducing the experimental and theoretical techniques, we discuss characterization of the tip using theoretical analysis of experimental frequency detuning versus distance curves. Then we present theoretical results and a series of experimental images and demonstrate how atomic scale contrast features change as a function of the tip–surface distance. We describe and interpret these changes qualitatively for the entire series of images, and then pick one of the images for a quantitative statistical analysis and comparison with theory. In the following section we present calculated images and scan lines, and discuss the origin of image features on the basis of theoretical modelling.

2. Methods

2.1. Experimental techniques

Experiments were performed on a commercial, highest-quality fluoride single crystal with a surface prepared by cleavage along the (111) plane in ultrahigh vacuum (UHV) at a base pressure in the low 10^{-10} mbar range. After waiting for several hours for charge relaxation, the crystal was transferred in vacuum to the scanning force microscope (Omicron UHV-STM/AFM). The influence of residual surface charges was minimized by applying a bias voltage between the conducting SFM tip and the metallic plate supporting the crystal at the back.

Measurements were performed with a SFM operated in the dynamic mode [13]. The basic instrumentation and experimental techniques are similar to those used in our previous work [6] except for the introduction of a new digital demodulator for detecting the cantilever resonance frequency detuning (NanoSurf easyScan). This provided an improvement in signal/noise ratio of about one order of magnitude in comparison to previous measurements and eliminated any drift in the frequency detuning signal. A commercial (Nanosensors) silicon cantilever (77 kHz

resonance frequency, 6 N m^{-1} spring constant) was excited to oscillation at its resonance frequency with an amplitude of either 35 nm or 18 nm kept constant by a regulation loop.

We operated the SFM system at a high scanning speed of typically 50 nm s^{-1} and an extremely small gain for the distance control loop. This procedure is an approximation to the constant-height mode in the sense that coarse variations in tip–surface distance, e.g. due to misalignment between the sample surface plane and the plane of scanning, are compensated while fully preserving variations of the frequency detuning on the atomic scale. Therefore, in our scanning results, we display cantilever resonance frequency detuning rather than topographic data. We found that for the high oscillation amplitudes which we use, this mode of operation reveals more clearly the subtle features of the tip–surface interaction than the constant-frequency-detuning mode used in our previous studies [4, 6]. These subtle features are the basis for the image analysis and conclusions presented here.

For a clearer display, the original data have been processed by a low-pass Fourier filter and in some cases a box reject filter removing stripes parallel to the scanning direction before presentation in the figures. Care was taken to ensure that all features discussed here can be recognized in both processed images and the more noisy original data. Scan lines presented in figure 8 and figure 9 are cross-sections along the [121] directions of the images obtained from the processed data without any further averaging. We checked that they well represent the properties of the respective images and that apparent variations in details of the scan lines do not affect any of the conclusions drawn from the data. The details of data analysis and the way of extracting quantitative information from experimental images are discussed in section 5.2.

As has been shown in reference [14], analysis of experimental frequency detuning curves as a function of the tip–surface distance can help to determine the interrelation between the main mesoscopic forces (such as van der Waals, capacitance and electrostatic force due to tip and/or surface charging), which contribute to the so-called 'background' force. The background force determines the average frequency detuning during scanning, whereas the relation between different constituent forces contains information about tip shape, composition and charge [15].

To characterize our tips we used the following procedures. Immediately after taking the last image of the series (shown as figure 7), the distance control loop was switched off and the vibrating tip retracted in a controlled way at a fixed lateral position. Frequency detuning data were sampled for five seconds; during that time the tip was retracted by 10 nm. After taking this measurement, we changed the amplitude of the tip from 35 nm to 18 nm and recorded another set of atomically resolved images which are not shown here and afterwards again a frequency detuning versus distance curve as described above. Lateral thermal drift of the sample, which is unavoidable at room temperature, does not allow precise tip positioning over a specific ionic site. Therefore, our data represent an average over a spread of lateral positions. However, as the force curves are analysed only with respect to long-range forces, this uncertainty does not affect the conclusions presented below. Finally, we should note that by following the piezo-control voltage, the relative movement of the cantilever base during the retraction is measured precisely, but the absolute tip–surface distance cannot be determined.

Atomic contrast in SFM images is determined by the details of the atomic structure at the end of the tip. Therefore cleaning, sharpening and modification of Si tips are important issues but not well understood so far. It has been demonstrated that field emission microscopy allows structural characterization of the tip on the atomic scale [16]; however, such characterization is not yet applied routinely and a correlation between the structure of well characterized tips and high-quality atomic resolution imaging has not yet been demonstrated to our knowledge. In our case, tips were not sputtered and hence were coated by native oxide, hydroxide and possibly other species of unknown composition. Furthermore, we found that it is favourable for atomic

resolution imaging on fluorides to bring the tip into slight contact with the surface prior to taking images in the dynamic mode. This method of tip preparation was also performed prior to the experiments reported here and it is likely that the tip has picked up surface constituents during this procedure.

2.2. Theoretical method

The model used in this study is the same as that described in references [9] and [17]. Hence, in this section we will only summarize the main features and focus in detail only on aspects of the modelling that are specific to this study. A schematic diagram of the tip and surface set-up used in the calculations is shown in figure 1. We assume a conducting tip having a conical shape on the macroscopic scale with a sphere of radius r at the end. We also assume that the end of the tip is ionic, stoichiometric and atomically sharp. Our previous extensive modelling [11] demonstrates that if the tip is not stoichiometric, it is very likely to pick up another surface ion and compensate the charge. The fact that several images were obtained with the same tip is a strong indication that the tip structure is stable, and since there are no shadows and other indications of a multi-tip or blunt tip, the assumption that the tip apex is atomically sharp seems reasonable. This implies that what really matters are the sign and gradient of the electrostatic potential at the probing end of the tip. To represent this potential, the tip is terminated by an oxide cluster in the form of a 64-atom MgO cube embedded into the macroscopic tip. This has been shown previously [10, 11] to well represent the potential of oxidized or contaminated silicon tips and ionic clusters. The cube is orientated so that it is symmetric about the z-axis with either a single oxygen or magnesium ion at the lowest point of the tip.

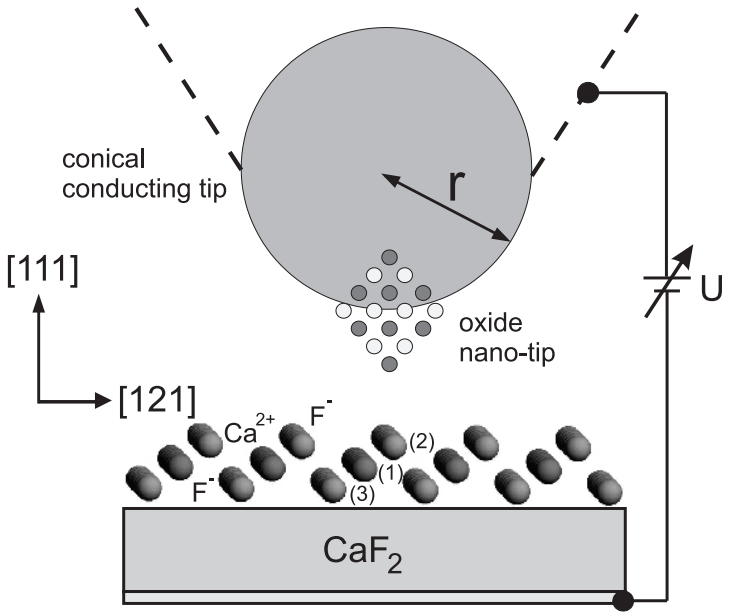

Figure 1. A schematic picture of the model used to simulate the interaction between the tip and the sample. r is the effective radius of the macroscopic tip and U is the bias voltage applied between the conducting tip and the conducting substrate. The nano-tip is a schematic representation of the 64-atom MgO cube used. Numbers in parentheses refer to ionic layers mentioned in the text.

The tip–surface interaction in our model includes three main components:

(i) the *microscopic* chemical force between the tip atoms and the surface, including the van der Waals force between ions;
(ii) the *macroscopic* van der Waals force between the tip apex and the surface; and
(iii) the electrostatic force due to work functions, charging and polarization of conducting materials.

Their relative contributions depend on the specific tip–surface combination studied. To integrate macroscopic and microscopic interactions in the same model we used the approach described in references [9] and [18]. The macroscopic van der Waals and image force comprise a *background attractive force*, which is important for reproducing experimentally observed *average* frequency changes. Small variations of frequency detuning on the atomic scale are largely determined by microscopic interactions. Therefore, these interactions can be calculated separately and just combined for the final stages of modelling. In the theoretical scan lines and images shown in the next section, the macroscopic force is included by calculating the image force and macroscopic van der Waals force, and then adding them to the microscopic force as a function of tip–surface distance to compute the total force. Note that although the individual components of the total force may be repulsive, images are taken at tip–surface separations of 0.4–0.8 nm where the overall force is *always* attractive. The balance between van der Waals and electrostatic forces depends on the specific separation, with electrostatic forces dominating at 0.4–0.5 nm and van der Waals dominating beyond 0.6 nm. However, atomic resolution in ionic systems is always dominated by the electrostatic interaction between tip and surface ions, as the van der Waals force is effectively uniform at a given tip–surface separation.

The distance dependence of the van der Waals force is calculated using the method described in reference [19]. A Hamaker constant, which according to the Lifshitz theory depends on the tip and surface electronic structure, was estimated to be equal to 1 eV using data found in reference [19]. We note that this is an average number which is characteristic of the interaction between semiconductor and insulator. Its more precise determination is difficult. It enters the expressions for the van der Waals force in a product with the effective tip radius, which is in most cases unknown. Therefore, instead of varying both parameters, in our further analysis we tried to estimate only the tip radius.

The microscopic force is calculated using a periodic static atomistic simulation technique and the MARVIN2 code [20]. The empirical parameters used for the tip, CaF_2 surface and tip–surface interactions are the same as in reference [17]. The unit cell used in the simulations to represent the CaF_2 surface is equivalent to extending the single layer shown in figure 1 three times in both the lateral and vertical directions. The bottom of the nano-tip and the top of the CaF_2 surface (top two layers) are relaxed explicitly in the same way as in previous studies [9]. The tip is virtually scanned across the surface at a range of tip–surface separations to generate a force grid $F(x, y, z)$.

The next stage of the modelling is to calculate the oscillations of the cantilever under the influence of this tip–surface force. The oscillations of the cantilever over a surface point (x, y) driven by an external force in a force field $F(z)$ can be described by the equation of motion:

$$\ddot{z} + \omega_0^2 z - \frac{\omega_0^2}{k} F(z + h) = 0 \tag{1}$$

where ω_0 is the resonance frequency of the cantilever in the absence of any interaction with the surface, k is the spring constant of the cantilever and h is the equilibrium height of the cantilever above the surface in the absence of interaction. Any interaction of the tip with the surface will cause a detuning of the resonance frequency ω_0 to ω; however, as the tip oscillations are maintained at constant amplitude, we can assume that any damping is completely compensated

by an external force and that $F(z)$ does not depend on time. On searching for a solution in the form of a Fourier series [9], the normalized frequency of the cantilever oscillations in the presence of the interaction $\Omega = \omega/\omega_0$ is obtained as

$$\Omega^2 = 1 - \frac{1}{\pi k A_1} \int_0^{2\pi} F(z + h) \cos(\tau)\, \mathrm{d}\tau. \tag{2}$$

A similar result was derived by Giessibl [3] using perturbation theory and a more specific force expression, but equation (2) represents a more general form.

Since the experimental images and scan lines presented in this study were produced via the 'constant-height' mode of dynamic mode SFM, simulated images and scan lines were calculated in the same manner, with an interpolation of the calculated detuning for a given tip–surface separation generating the image. All calculated force curves and scan lines were produced assuming a cantilever amplitude of 35 nm or 18 nm, a resonance frequency of 77 kHz and a spring constant of 6 N m^{-1}, according to the experimental parameters.

3. Tip and surface characterization

The average resonance frequency detuning during imaging is determined primarily by the background force, whereas image contrast results from small variations of detuning due to the short-range chemical interaction between tip and surface. The main contributions to the background force are long-range electrostatic forces due to residual surface charges and long-range van der Waals forces depending on the composition, radius and shape. As has been demonstrated in reference [15], analysis of the forces measured on the tip as a function of the tip–surface distance at different values of the external bias voltage can provide numerical values of the parameters of these interactions, such as the effective tip radius. These values can then be used as input for theoretical simulations of SFM images. In this section we discuss the analysis of background forces performed in this work.

It is common practice to minimize long-range electrostatic interactions by applying a bias voltage, a procedure similar to that described in reference [21], and this was used in all measurements presented here. The compensating bias voltage exhibits strong variations from one cleave to another and smaller variations when probing different locations on the surface. We find a range of values between −10 V and +4 V. All experimental results presented below have been obtained with a compensating bias voltage of +3.3 V.

The measured frequency detuning curves strongly depend on tip preparation. For further analysis we have chosen the curves shown in figure 2 obtained with two different tips. The first tip is a standard unsputtered tip which will be referred to as the 'sharp tip'. The second tip was prepared by effectively crashing the sharp tip to produce a much blunter tip referred to as the 'blunt tip'. Distances given in the graphs of figure 2 have been obtained by shifting experimental data to align with theoretical curves assuming that closest approach of the tip to the surface occurs at 0.4 nm. This is an estimate which is based on the results of theoretical modelling of the tip–surface interaction [17]. We found that 0.4 nm is a typical tip–surface distance at which surface (tip) ions start to exhibit strong displacements from their equilibrium sites and may adsorb on the tip (surface) as they separate [9, 22]. At shorter distances, perturbations in the tip–surface interaction due to tip contamination by surface ions may lead to instabilities in cantilever oscillations. As these instabilities were not observed in our measurements, it was assumed that the tip–surface distance did not exceed this critical value.

For each of the tips, we measured the force curve for two oscillation amplitudes of 35 nm and 18 nm. The larger amplitude value was used for measurements shown here and the smaller one was included for comparison. Force curves for the larger amplitude show stronger

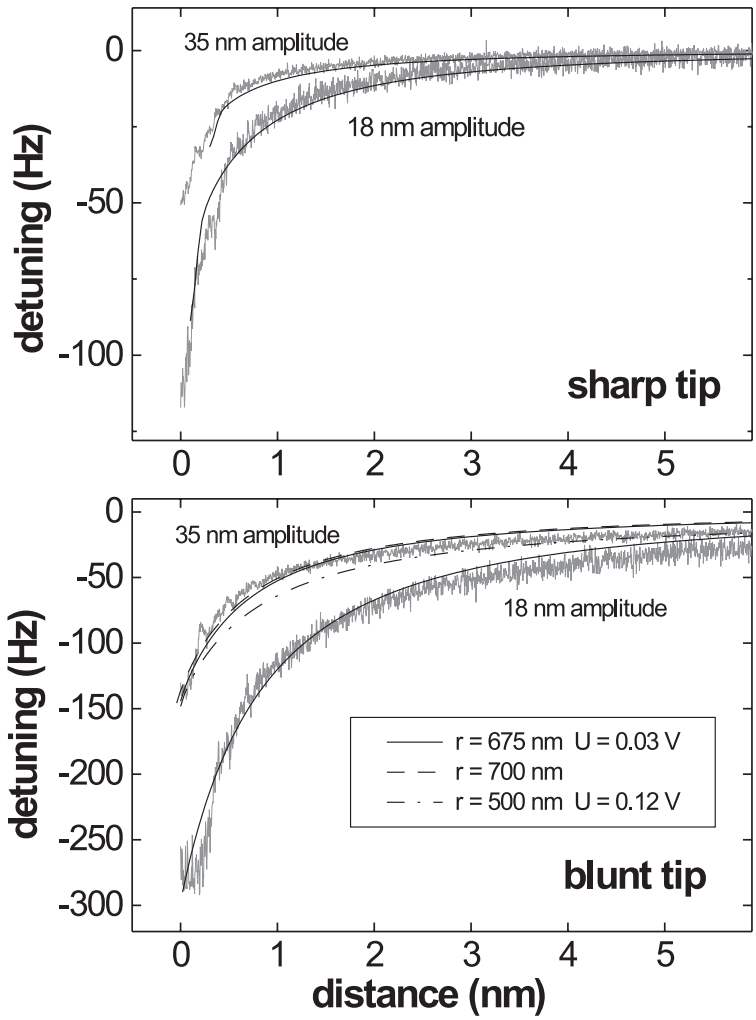

Figure 2. Comparison of theoretical and experimental detuning versus distance curves taken over the CaF_2 surface with two different tips and two different amplitudes. The sharp tip represents a standard unsputtered SFM tip. The blunt tip was produced by crashing the sharp tip into the surface.

dependence on distance than those for the smaller amplitude. From a series of measurements not shown here, it is generally found that the maximum frequency detuning at small distances roughly scales with amplitude as $\delta f \sim A^{-3/2}$, which is in accordance with the prediction from reference [23].

The experimental and theoretical force curves presented in figure 2 demonstrate a clear dependence on the tip shape. In particular, the tip–surface interaction is much more short-range for the sharp tip than for the blunt tip. The experimental curves are generally monotonic and smooth. However, at a distance range shorter than about 0.5 nm the slope for the sharp tip is much steeper than that for the blunt tip.

Using the SFM model described above, we have fitted theoretical curves to experimental data obtained at both oscillation amplitudes for the sharp as well as the blunt tip. The free

parameters of the fit were the tip radius and the bias voltage. The macroscopic van der Waals force between the tip and surface is proportional to the tip radius. The bias voltage applied in the theoretical model affects long-range electrostatic forces due to uncompensated surface charge and image interaction [15]. The best-fit results are shown as solid lines in the graphs of figure 2. The tip parameters for the fit are the same at both amplitudes, confirming that theory gives a consistent agreement.

For the sharp tip, the theoretical best fit was found for a tip radius of 100 nm and 0.0 V bias voltage. For the blunt tip the best fit was found for a tip radius of 675 nm and 0.03 V bias voltage. It should be noted that these parameters are quite unique and a similar fit could not be found with an increased bias and reduced radius. This is due to the very different behaviour of van der Waals and electrostatic forces as a function of distance [17]. In both cases the macroscopic van der Waals force dominates the interaction and the long-range electrostatic force due to bias is insignificant. The latter is consistent with the fact that the fitting was made to the curves obtained under the conditions where electrostatic forces have been minimized by the applied bias voltage.

The overall agreement between theoretical and experimental curves at long range is better for the sharp tip than for the blunt tip. A tip radius above 500 nm appears unrealistically large even for a blunted tip. This is not surprising taking into account the idealized tip model used in the calculations. In particular, the blunt tip can be expected to have an irregular shape with a number of nanoscale structures. These nanostructures will have overlapping ranges of interaction with the surface, determining the overall shape of the force curve by superposition and causing deviation of force curves from what would be expected from an ideally spherical tip end. Nonetheless, the parameters obtained are meaningful input values for theoretical calculations since by using them for calculating the background forces, the absolute values for the frequency detuning of theory and experiment can be aligned with each other. The choice of the tip radius and the associated compensating bias voltage, however, does not affect the interpretation of contrast on the atomic scale where the interactions of surface ions with the atomic cluster at the tip end are dominant [17].

Since the atomically resolved images of highest quality were produced with the blunt tip, only experimental results obtained with that tip will be discussed further. This also means that all theoretical images and scan lines have been calculated using a macroscopic tip of radius 675 nm and an applied bias of 0.03 V.

4. Theoretical results

Since the detailed structure of tips used in experiments is not known *a priori*, we performed calculations with both a nano-tip terminated with an anion and a cation-terminated tip. This simulates imaging with a tip that has a microscopic atomic composition producing negative and positive electrostatic potentials, respectively. Results are represented in two different ways, namely as two-dimensional images displaying the detuning as a function of surface position and as scan lines along the [121] direction that is distinguished in so far as the plane of this scan line centrally intersects anions from both fluorine sublattices as well as cations from the calcium sublattice. Images were generated by calculating the frequency detuning over a grid of 15 points in an irreducible part of the surface unit cell and then symmetry was used to create an image of the whole cell. This was then repeated according to the surface lattice vectors to generate points across a larger extension of the surface. Finally, for a better visualization, linear interpolation was used between calculated points to produce the simulated image. Simulated scan lines show a sequence of calculated points along a given

direction without any interpolation. As reference points, we marked anion and cation sites of the topmost three layers in simulated images as well as scan lines. We associated the number (1) with the calcium sublattice while the upper and lower fluorine sublattices are labelled by numbers (2) and (3), respectively (see figure 1).

4.1. Anion-terminated tip

First simulations were performed with the nano-tip orientated so that an O^{2-} ion was at the apex, yielding a negative potential at the end of the tip. For comparison with experimental images, where the absolute height is unknown, the average frequency detuning over the entire image can be taken as an effective measure of tip–surface distance. The more closely the tip approaches the surface, the stronger the overall attractive force and, consequently, the larger the magnitude of the average frequency change. Therefore, tip–surface separations used in the theoretical studies were chosen to cover the range of average detunings seen in experimental images.

Figure 3 shows three simulated images taken at different tip–surface separations. Images are orientated such that the horizontal white line is along the direction [121]. The average frequency change in the images in figure 3 was chosen to be -121 Hz (A), -129 Hz (B) and -139 Hz (C). In figure 3, maximum brightness, corresponding to the largest magnitude in detuning, in simulated images appears above Ca^{2+} sites. Additionally, a slight increase in brightness can be seen halfway between the bright spots along the [121] direction. The images demonstrate a clear qualitative change in contrast as the tip moves closer to the surface. The bright spots seen at 0.5 nm distance are non-circular, but upon closer approach, the spots become more circular until they are almost perfect discs at a distance of 0.4 nm. The change in images as a function of tip–surface separation can be analysed more quantitatively by comparing scan lines. Figure 4 shows three simulated scan lines taken at different tip–surface separations, along the white line shown in figure 3. These, and all other simulated scan lines, have been scaled so that the minimum detuning in the scan line is set as the zero-detuning point. As expected from the images, the simulated scan lines exhibit a secondary maximum between the two F^- ions at 0.33 nm from the main peaks.

Relating images and scan lines to the ionic positions indicated allows an interpretation of the contrast features. The large maxima correspond to calcium sites and are due to strong attraction of the negative tip by the cations. The minima appear at sites of maximum repulsion over F^- ions. The weaker repulsion over the deeper F(3) ion compared to the protruding F(2) ion is reflected in a shallower scan-line minimum and the small maximum in between marks the intermediate point of minimum repulsion. This makes the maximum peaks, primary and secondary, asymmetric and translates directly into the simulated images as a slower decay of brightness on one side of Ca^{2+} ions. This gives the spots over the Ca^{2+} ions a weak triangular shape at greater tip–surface separations.

Figure 4 clearly shows the dependence of the magnitude of the contrast on the tip–surface separation. At 0.5 nm the contrast over the Ca^{2+} ions is about 0.2 Hz, whereas at 0.4 nm it is about 1.8 Hz. As the tip moves closer to the surface, the chemical forces between the atoms in the surface and the tip increase, producing a corresponding increase in contrast. Surface relaxation also plays a role in the interaction, with the Ca ions displacing towards the tip by about 0.01 nm during scanning and actually jumping to the tip at tip–surface separations of less than 0.38 nm. The displacement of the ions causes a small increase in contrast while scanning due to an increase in the range of the electrostatic potential from the displaced ion [7]. The scan lines show an increase in contrast at the secondary maximum as the tip–surface separation is reduced. At 0.5 nm it is about 0.05 Hz and at 0.4 nm it is about 0.2 Hz. However, this

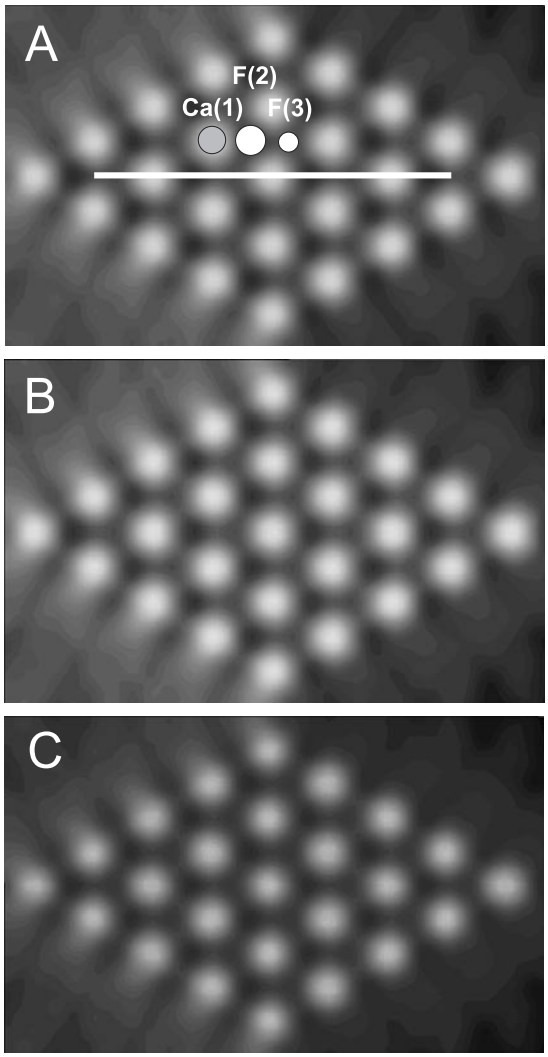

Figure 3. Simulated frequency change images at constant height over the $CaF_2(111)$ surface with an oxygen-terminated nano-tip. The images are labelled according to height: A: −0.50 nm; B: −0.45 nm; C: −0.40 nm. The numbers above the ionic positions refer to the labels in figure 1. The white line along the [121] direction denotes the positions of the scan lines shown in figure 4.

means that it decreases in significance from about 0.22 to 0.11 Hz as a fraction of the contrast over the Ca^{2+} ions in the same distance range. As the tip is moved closer to the surface, the contrast over the Ca^{2+} ions gets larger, and eventually the difference in contrast over the two F^- sites is so small compared to contrast over the Ca^{2+} sites that it is irrelevant. Effectively only the interaction over Ca^{2+} ions is seen in images and, as this is symmetrical, the spots become circular. This is because the repulsive interaction with the singly charged F^- ions producing the secondary maximum has a weaker distance dependence than the direct attractive interaction over the Ca^{2+} sites. It should be noted that all the same interactions are present at every tip–surface separation, but it is the change in their relative magnitude as a function of distance that causes a qualitative change in the apparent images.

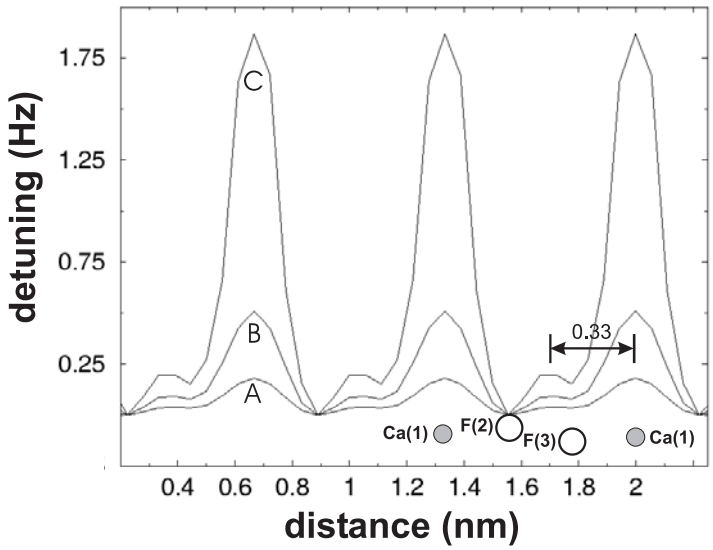

Figure 4. Simulated frequency change scan lines at constant height over the $CaF_2(111)$ surface along the [121] direction with an oxygen-terminated nano-tip. The scan lines are labelled according to height: A: −0.50 nm; B: −0.45 nm; C: −0.40 nm. Height is measured with respect to the Ca^{2+} sublattice (1).

4.2. Cation-terminated tip

Simulations in this section were performed with the nano-tip orientated so that a Mg^{2+} ion was at the apex and the tip end had an effective positive potential. In analogy to results presented in the previous subsection, figure 5 shows three simulated images taken at different tip–surface separations. The average frequency change for each image was chosen to be −121 Hz (A), −129 Hz (B) and −139 Hz (C). In figure 5, maximum contrast in the simulated images is over the F(2) sites (see figure 1). The contrast pattern in the images is consistently triangular at all tip–surface separations but this shape can most clearly be recognized in the image representing the smallest tip–surface distance.

As before, we analyse this behaviour more quantitatively by taking scan lines from the images. Figure 6 shows three simulated scan lines taken at different tip–surface separations, along the white line shown in figure 5. As in the scan lines for the O^{2-}-terminated tip, a shoulder can be seen. However, now it is found at 0.22 nm next to the main peak. The shoulder strongly elongates the contrast feature over the F(2) ions in the [121] directions, producing the characteristic triangular shape. Again, figure 6 clearly shows the dependence of the magnitude of the contrast on the tip–surface separation. While scanning, the F ions displace by about 0.02 nm towards the tip and jump to the tip at tip–surface separations of less than 0.40 nm. At 0.5 nm the contrast over the F^- ions is about 0.25 Hz, whereas at 0.4 nm it is about 3.0 Hz. The shoulder on the main peaks due to this interaction increases in size as the tip moves closer; at 0.5 nm it is about 0.1 Hz and at 0.4 nm it is about 0.8 Hz. However, unlike the secondary maximum in figure 4, even at 0.4 nm the shoulder is still a significant fraction of the contrast over the F(2) ions. It only decreases from 0.46 at 0.5 nm to 0.27 at 0.4 nm. This is due to the different origin of the contrast features in this case. Both maxima are now due to attractions between F^- ions and the tip apex ion and, therefore, primary and secondary features effectively exhibit the same distance dependence. The images in figure 5

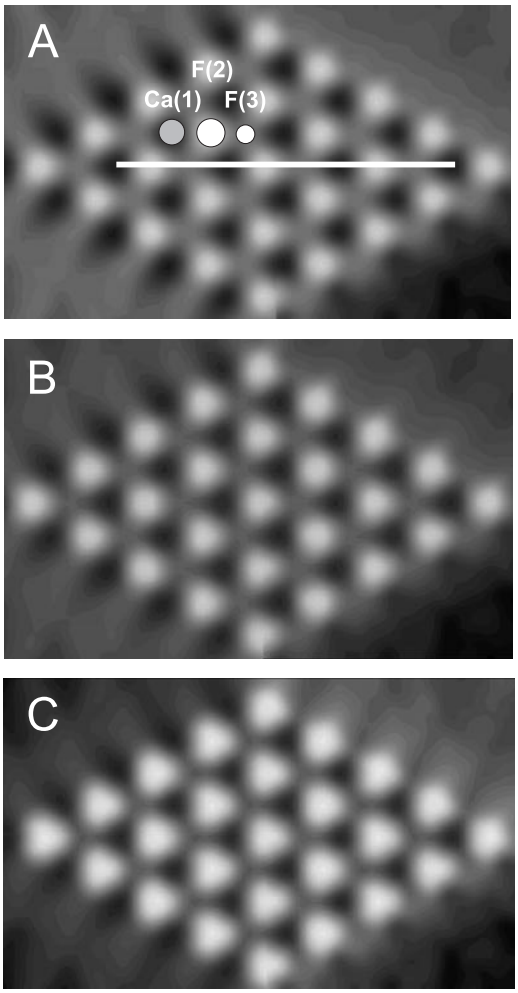

Figure 5. Simulated frequency change images at constant height over the $CaF_2(111)$ surface with a magnesium-terminated nano-tip. The images are labelled according to height: A: −0.50 nm; B: −0.45 nm; C: −0.40 nm. Numbers above the ionic positions refer to the labels in figure 1. The white line along the [121] direction denotes the positions of the scan lines shown in figure 6.

directly reflect the significance of the shoulder at all tip–surface separations; even at 0.4 nm the bright spots are clearly triangular due to the convolution of the interactions of the tip with both F^- sites.

5. Experimental results

5.1. Basic features and conclusions

A series of atomic resolution images of a 4×4 nm^2 surface area on a flat terrace is shown in figure 7. The mean frequency detuning increases from −121 Hz through −127 Hz to −140 Hz from the upper to the lower frame in the series. Frames grouped on the left-hand side represent forward scans and those on the right-hand side the corresponding backward scans sampled

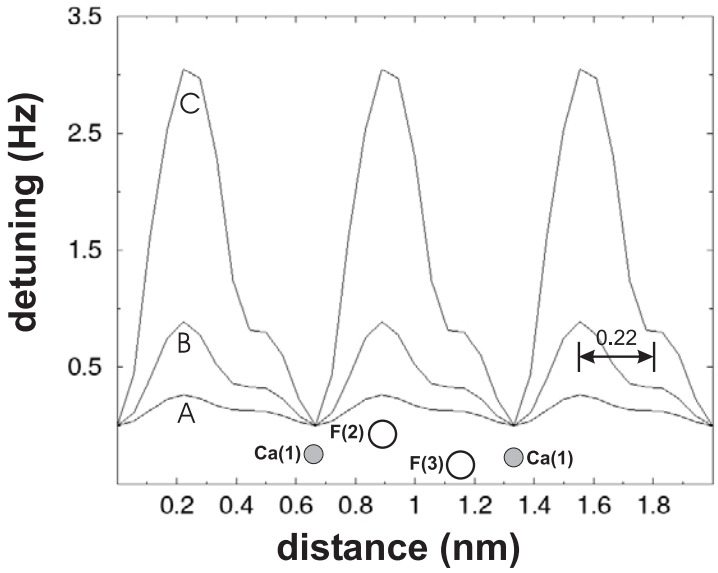

Figure 6. Simulated frequency change scan lines at constant height over the $CaF_2(111)$ surface along the [121] direction with a magnesium-terminated nano-tip. Scan lines are labelled according to height: A: −0.50 nm; B: −0.45 nm; C: −0.40 nm. Height is measured with respect to the Ca^{2+} sublattice (1).

immediately after each other. Scan lines along the [121] direction, taken as indicated by white lines in figure 7, are shown in figure 8.

The forward and backward images A and B representing the lowest frequency detuning in figure 7 exhibit a clearly triangular shape of the bright spots. Analysis of corresponding scan lines in figure 8 demonstrates that the apparent triangular structure of image features is due to two distinct maxima along the [121] direction. These results are in qualitative agreement with theoretical predictions for a Mg^{2+}-terminated tip but not for the tip with O^{2-} termination.

Frames and scan lines C in figures 7 and 8, respectively, demonstrate a completely different pattern. They correspond to a larger frequency detuning and consequently to a smaller tip–surface separation at the lowest point of tip oscillations than images A and B. Looking at figure 8, it is obvious that the system behaves differently for scanning in forward and backward directions. Our measurements show in the forward scanning direction (C) bright spots which merge into a honeycomb pattern surrounding deep 'holes' of very small frequency detuning. However, as the tip moves in the backward direction a pattern of enhanced stripes in the [110] direction is visible. These images may result from an interplay of several complex factors, such as multiple nano-tip structure of the blunt tip and strong displacements and rearrangement of ions on the tip at short tip–surface distances. The fact that such rearrangements can happen periodically has been demonstrated in previous molecular dynamics simulations [22]. However, we believe that neither better tip characterization nor more sophisticated theoretical modelling would provide a reliable and satisfactory explanation of these images beyond speculations. Therefore, they clearly demonstrate the limitations of available techniques both in terms of tip preparation and determination of the tip–surface separation.

Since the tip–surface interaction is highly non-linear, tip and cantilever response critically depend on subtle variations in the interaction potential. Therefore, the qualitative agreement between theory and experiment both in terms of the shape of image features and the systematic

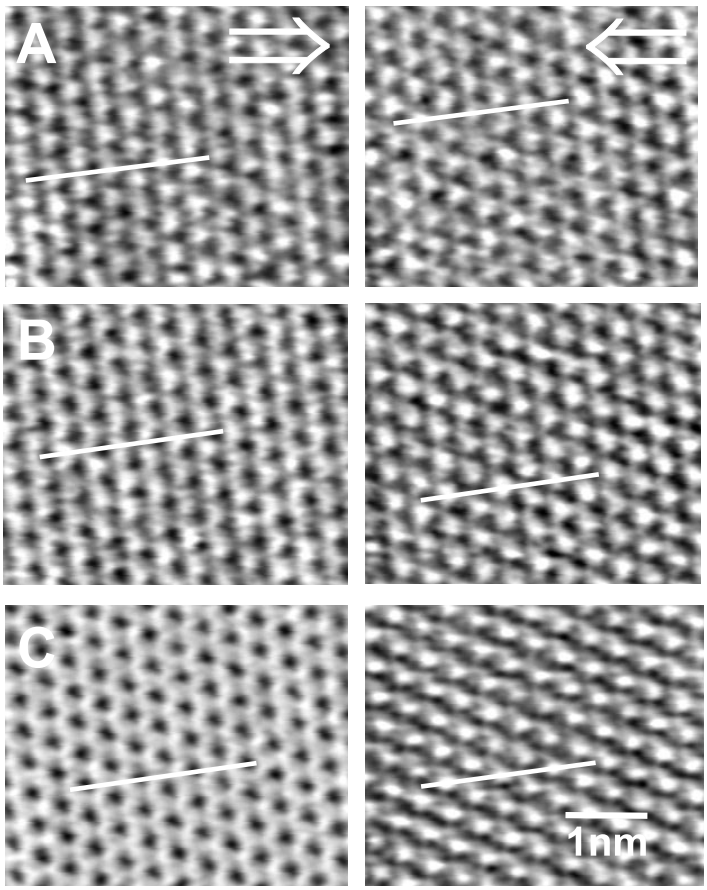

Figure 7. Detuning recorded in the constant-height mode for forward (left-hand column) and backward (right-hand column) scanning direction. From row A to row C the frequency detuning was lowered from −121 Hz to −127 Hz and −140 Hz. The white lines represent the positions of the detuning scan lines shown in figure 8.

change in their shape in frames A and B obtained for smaller frequency detuning may be not entirely superficial. This agreement suggests that the end of the tip used in these experiments could be characterized by a positive electrostatic potential similar to that corresponding to our idealized tip terminated by a positive ion. Consequently, bright features can be interpreted as corresponding to fluorine sites of the first and second anion sublattices, respectively, while the dark spots in between define the positions of Ca^{2+} ions from the cation sublattice. To test these conclusions, in the next section we make a quantitative comparison of experimental and theoretical scan lines.

5.2. Quantification and comparison to theory

Quantitative comparison between SFM experiment and theory requires elucidation of several crucial issues. First, experimental images should be treated using standard procedures of image analysis like filtering, averaging and removal of distortions. Lateral positions of image features can be influenced by drift and noise. Therefore, average scan lines should have statistical errors

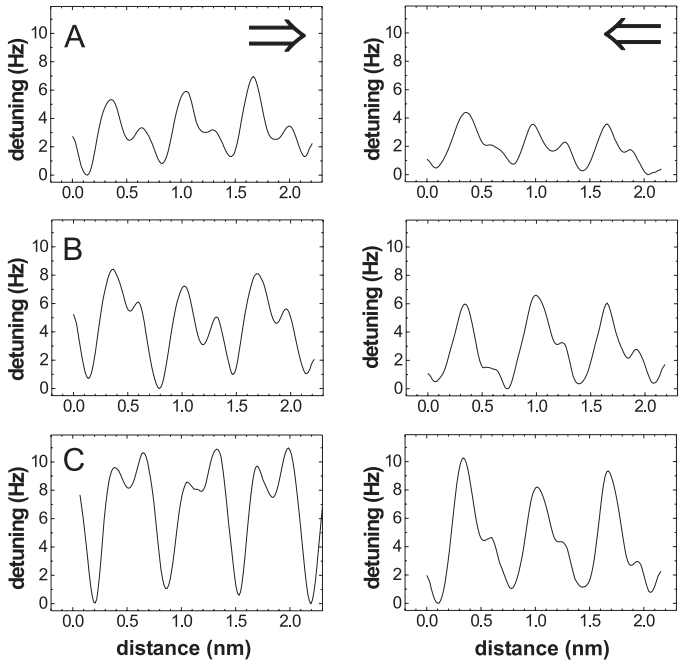

Figure 8. Frequency change scan lines in forward (left-hand column) and backward (right-hand column) scanning directions extracted from the Fourier-filtered images of figure 7. Labels A, B and C correspond to the labels of figure 7.

determined for the most characteristic features, such as distances between different maxima and their relative height and width. Another issue concerns the shape of the tip, its chemical structure and atomic composition at the end, which currently cannot be reliably established. Some information can be obtained by sequentially imaging the same surface area with the same tip at different frequency detunings. If at small detunings the image pattern does not change significantly from frame to frame, one can reasonably assume that the tip structure remains stable and is determined by one relatively sharp nano-asperity. Theoretical results [7] demonstrate that blunt nano-tips would not yield atomic resolution.

Yet another issue concerns which theoretical images to compare with experiment. Ideally, the two images should correspond, for example, to the same tip–surface distance. However, so far, there is no way of reliably determining this distance from the experiment. If idealized tips used in theory closely represented the real tips used in experiment, the tip–surface distance could simply be derived by fitting theory to scanning results and one would obtain a unique solution. Due to the uncertainty in the actual tip structure, however, such a fit cannot be expected to yield a reliable result. In both experiment and theory, we observe the expected dependence of image contrast on the tip–surface distance. The contrast increases when reducing distance and, in the distance range that appears to be feasible for atomic scale imaging, results coincide within the same order of magnitude. However, only if the real tip itself was effectively 'ideal' could a quantitative comparison of the magnitude of contrast in experiment and theory be used to accurately give the absolute tip–surface separation in experiments.

In spite of these uncertainties we continue with our image analysis in order to determine whether reliable quantitative information can be extracted from experimental data. For the analysis we pick frame B from figure 7 since it has the highest quality. Image processing

comprises several steps of Fourier filtering, line selection and line averaging that are visualized in figures 9 and 10. Figure 9 shows two rows displaying original data on the left-hand side and Fourier-filtered data on the right-hand side, respectively. The three graphs below the images at the top of each row represent scan lines taken along the three equivalent [121] directions on the surface. Figure 10 displays power spectra obtained after applying a two-dimensional Fourier transformation to the original image from the experiment and then applying the same transformation to the corresponding theoretical image (frame C in figure 5). In figure 10, we also indicate the positions of the filter elements applied in Fourier space to obtain smoothed images and scan lines from the original data.

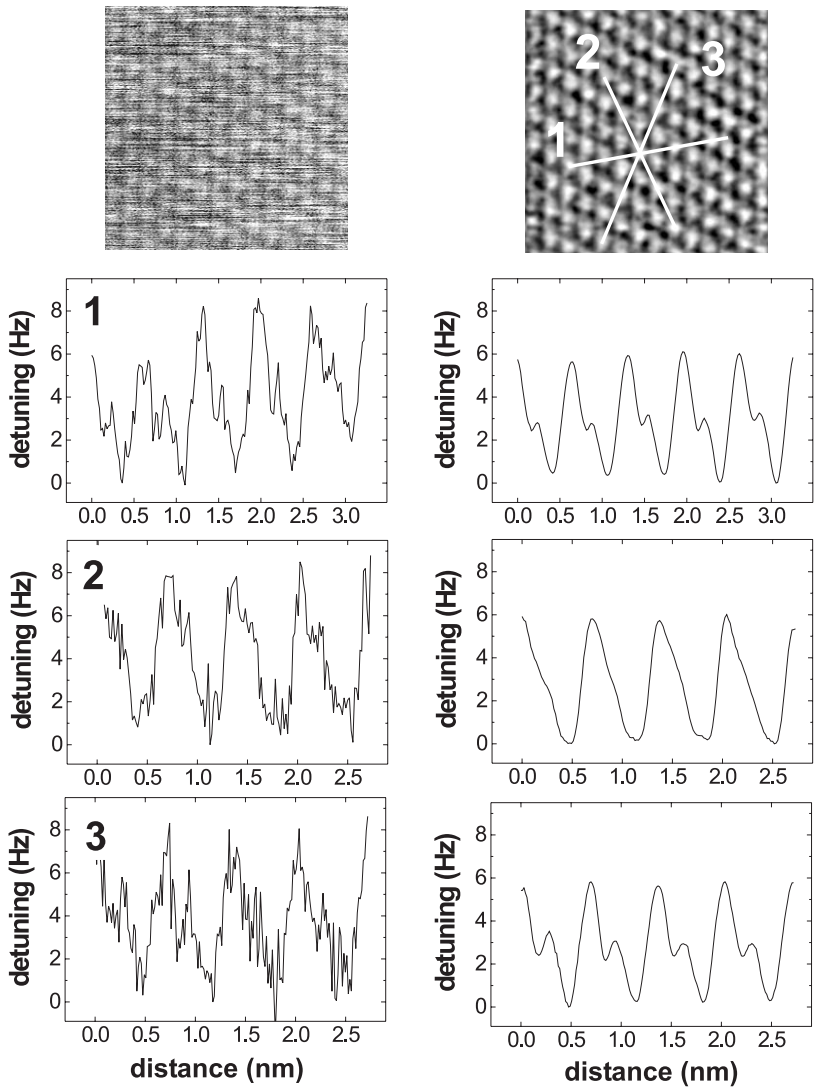

Figure 9. Detuning images representing the original (left-hand side) and Fourier-filtered and averaged data (right-hand side) of frame B (backward) from figure 7. Scan line profiles were taken along the three equivalent [121] directions. Details of averaging and Fourier filtering are discussed in the text.

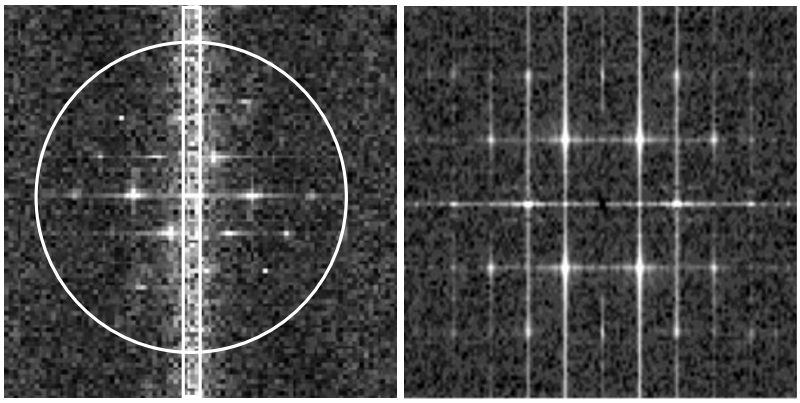

Figure 10. Power spectra after a 2D Fourier transformation of the experimental image (left frame) shown in figure 9 and the theoretical image (right frame) shown in figure 5 (frame C). The white circle and narrow box in the experimental image represent a low-pass filter with radius $r = 7.0\,\mathrm{nm}^{-1}$ and a box reject filter, respectively. The dimensions of the power spectra are $8.3 \times 11.3\ \mathrm{nm}^{-2}$ (left) and $6.8 \times 6.8\ \mathrm{nm}^{-2}$ (right).

A comparison of Fourier spectra from figure 10 reveals that the experimental image contains the main features predicted by theory; i.e. a symmetric array of six peaks centred around the origin. The images are in good agreement with each other as regards the relative positions of the peaks while the spectrum of the experimental image appears to be somewhat rotated, which is due to the inclination of the scanning direction with respect to the [121] axis by about 9°. The main sources of noise, apparent in the experimental spectrum are random noise, yielding power in the entire plane of the reciprocal space, and random stripe patterns in the fast-scanning direction, yielding power concentrated on a vertical line intersecting the origin. To suppress both types of noise, we apply two types of filter. One is a low-pass filter, suppressing high Fourier components with frequencies larger than $7.0\ \mathrm{nm}^{-1}$, and the other is a box reject filter, suppressing features related to the fast-scanning direction. Since the latter filter, by definition, also suppresses power at zero spatial frequency and in the vicinity of the origin along all directions, it removes low-frequency fluctuations and effectively yields a plane correction. The effects of both filters can immediately be recognized when comparing filtered line scan lines with original scan lines in figure 9. The filtered scan lines exhibit considerably less high-frequency noise and are also much more even regarding the heights of equivalent maxima and minima.

The scan lines shown in figure 9 do not represent individual scan lines but have been obtained by averaging the maximum possible number of scan lines in each direction. The scan lines were obtained by the addition of 32, 30 and 26 scan lines along directions 1, 2 and 3, respectively, of 16, 15 and 13 parallel and equivalent ionic rows. Here, two adjacent scan lines are used for each ionic row. We find that the averaged original data clearly contain the two-peak structure with one peak being about half as high as the other. The fact that the secondary feature is present in the scan lines for all directions is a proof that it is not related to the fast-scanning direction. The detailed structures of the scan lines along the three directions are, however, different. While we observe a distinct second feature for directions 1 and 3, there is only a much weaker shoulder for direction 2. This can be attributed to the asymmetry of the tip-terminating cluster, yielding different interactions in equivalent directions. This imposes limitations for a quantitative comparison between experiment and theory since one cannot decide *a priori* which of the three experimental scan lines is the 'true' one to be

compared to theory. Taking an average of all three yields a scan line that is quite similar to the theoretically predicted scan line. However, one has to keep in mind that by this procedure, we do not average data superimposed with random noise, but average three curves having some systematic differences.

The most reliable parameter that can be extracted from the averaged scan lines of Fourier-filtered data is the relative distance between the main and secondary peaks in the images. For the directions 1 and 3 we find distances of 0.24 ± 0.03 nm and 0.26 ± 0.03 nm, respectively, which are slightly above the theoretical value of 0.22 nm. In the scan line along direction 2, the secondary peak is much less pronounced, so it is difficult to determine its position exactly. We estimate a distance of 0.19 ± 0.06 nm, which is slightly below the theoretical value. However, all three values and their mean value of 0.23 ± 0.04 nm are found to be within their errors equal to the theoretical value of the cation-terminated tip, demonstrating good agreement between experiment and theory. The height of the secondary peak is 2.1 ± 0.4 and 1.8 ± 0.4 times smaller than the primary peak along the directions 1 and 3, respectively—in comparison to theory, which predicts a secondary peak 3.7 times smaller at a tip–surface separation of 0.4 nm. However, this discrepancy is related to the difficulties, discussed previously, of establishing the real tip–surface separation in experiments and cannot be reconciled without greater knowledge of the tip.

6. Summary and conclusions

We believe that the comparison between experiment and theory discussed above provides better understanding of both experimental images and the limitations of the theoretical model. In particular, the theoretical analysis of experimental force curves showed that the tip–surface interaction in experiments was dominated by the van der Waals force and that electrostatic forces due to surface and/or tip charging were negligible. The model correctly predicted that the tip used in the experiment was blunt and that there were only tiny residual electrostatic forces due to the fact that they were compensated by the bias voltage applied in the experiment. The general consistency between theoretical and experimental images as a function of tip–surface separation supports the assumption that the tip–surface distance in experimental images is around the 0.45 nm mark predicted by theory. A more precise determination of the distance is, however, precluded by the unknown tip structure.

Both experiment and theory demonstrated that the contrast in images crucially depends on the nature of the tip. Modelling predicted that an anion-terminated tip with a negative potential would image the Ca^{2+} sublattice as bright and that the pattern of contrast would be rather disc-like at all tip–surface separations. For a cation-terminated tip with a positive potential, modelling predicted that the protruding F^- sublattice would be imaged as bright, producing a triangular pattern of contrast in images due to the interaction with the deeper F^- sublattice. The latter agrees with experiment and is supported by the quantitative comparison of the experimental and theoretical scan lines. The characteristic triangular pattern is due to the formation of the secondary peaks or shoulders in the scan lines. Theory predicts that these shoulders should appear at 0.22 nm from the main peaks and this agrees well with the experimental average position of 0.23 ± 0.04 nm. Moreover, both theory and experiment predict that the relative height of the primary and secondary maxima decreases as the tip moves closer to the surface.

This overall agreement yields convincing evidence that in experiment the tip had a positive potential and that the protruding F^- sublattice was imaged as bright with the deeper F^- sublattice producing the triangular contrast pattern. Although most tips are initially oxidized, yielding a negative potential at the tip end, having a positive potential is equally, if not more,

probable, since during tip preparation and also during the experiment, the tip can easily be contaminated by picking up positive species from the surface. This again points to the fact that the unknown atomistic structure at the end of the tip is the most severe restriction for quantitative interpretation of SFM images. Nevertheless the general agreement between experiment and theory supports our initial assumption that at tip–surface separations characteristic for dynamic SFM the sign and gradient of the tip electrostatic potential, rather than the detailed tip composition, plays the dominant role. The fact that a simple model of a stable, sharp, ionic tip, like a MgO cluster, can adequately represent the tip potential makes us optimistic as regards further quantitative comparison of theory and experiment, and interpretation of dynamic SFM images.

The results presented here have clearly demonstrated that we are now able to unambiguously identify sublattices on a binary insulator and semi-quantitatively understand all contrast features apparent in the images. In fact, we were able to sample data from the three topmost ionic layers of the insulator. Having now developed the instrumentation for an in-depth analysis of atomic corrugation on insulators, we expect that we will be able to extract even more specific information from insulating surfaces with a more complex structure. A fully quantitative understanding of SFM images obtained on their surfaces, however, requires tremendous efforts in obtaining control of the tip structure.

Acknowledgments

ASF acknowledges support from the EPSRC. Financial support by NATO CRG 974075 is gratefully acknowledged. We are grateful to R Bennewitz, F Giessibl and E Meyer for stimulating discussions and to A L Rohl for his help with the MARVIN2 code.

References

[1] Reichling M, Sils J, Johansen H and Matthias E 1999 *Appl. Phys.* A **69** S743
[2] Campbell C T 1997 *Surf. Sci. Rep.* **27** 1
[3] Giessibl F J 1995 *Science* **267** 68
[4] Reichling M and Barth C 1999 *Phys. Rev. Lett.* **83** 768
[5] Fukui K, Onishi H and Iwasawa Y 1999 *Phys. Rev. Lett.* **79** 4202
[6] Barth C and Reichling M 2000 *Surf. Sci. Lett.* **470** L99
[7] Bennewitz R, Foster A S, Kantorovich L N, Bammerlin M, Loppacher Ch, Schäfer S, Guggisberg M, Meyer E and Shluger A L 2000 *Phys. Rev.* B **62** 2074
[8] Raza H, Pang C L, Haycock S A and Thornton G 1999 *Appl. Surf. Sci.* **140** 271
[9] Livshits A I, Shluger A L, Rohl A L and Foster A S 1999 *Phys. Rev.* B **59** 2436
[10] Sushko P V, Foster A S, Kantorovich L N and Shluger A L 1999 *Appl. Surf. Sci.* **144+145** 608
[11] Shluger A L, Livshits A I, Foster A S and Catlow C R A 1999 *J. Phys.: Condens. Matter* **11** R295
[12] Foster A S, Barth C, Shluger A L and Reichling M 2001 *Phys. Rev. Lett.* at press
[13] Bammerlin M, Lüthi R, Meyer E, Baratoff A, Lü J, Guggisberg M, Loppacher C, Gerber C and Güntherodt H-J 1999 *Appl. Phys.* A **66** S293
[14] Guggisberg M, Bammerlin M, Loppacher Ch, Pfeiffer O, Abdurixit A, Barwich V, Bennewitz R, Baratoff A, Meyer E and Güntherodt H-J 2000 *Phys. Rev.* B **61** 11 151
[15] Foster A S, Kantorovich L N and Shluger A L 2000 *Appl. Phys.* A **72** 1
[16] Arai T and Tomitori M 1999 *J. Vac. Sci. Technol.* B **18** 648
[17] Foster A S, Rohl A L and Shluger A L 2001 *Appl. Phys.* A at press
[18] Kantorovich L N, Foster A S, Shluger A L and Stoneham A M 2000 *Surf. Sci.* **445** 283
[19] Argento C and French R H 1996 *J. Appl. Phys.* **80** 6081
[20] Gay D and Rohl A 1995 *J. Chem. Soc. Faraday Trans.* **91** 925
[21] Bennewitz R, Reichling M and Matthias E 1997 *Surf. Sci.* **387** 69
[22] Livshits A I and Shluger A L 1997 *Faraday Discuss.* **106** 425
[23] Giessibl F J 1997 *Phys. Rev.* B **56** 16 010